



Causes of a continuous summertime O₃ pollution event in Jinan, a central city in the North China Plain

Xiaopu Lyu¹, Nan Wang², Hai Guo¹, Likun Xue³, Fei Jiang⁴, Yangzong Zeren¹, Hairong Cheng⁵, Zhe Cai⁴,
Lihui Han⁶, and Ying Zhou⁶

¹Air Quality Studies, Department of Civil and Environmental Engineering,
the Hong Kong Polytechnic University, Hong Kong, China

²Division of Environmental Meteorology, Institute of Tropical and Marine Meteorology,
China Meteorology Administration, Guangzhou, China

³Environment Research Institute, Shandong University, Jinan, China

⁴Jiangsu Provincial Key Laboratory of Geographic Information Science and Technology,
International Institute for Earth System Science, Nanjing University, Nanjing, China

⁵Department of Environmental Engineering, School of Resource and Environmental Sciences,
Wuhan University, Wuhan, China

⁶Department of Environmental Science, College of Environmental and Energy Engineering,
Beijing University of Technology, Beijing, China

Correspondence: Hai Guo (ceguohai@polyu.edu.hk)

Received: 12 September 2018 – Discussion started: 27 September 2018

Revised: 31 December 2018 – Accepted: 20 February 2019 – Published: 8 March 2019

Abstract. In the summer of 2017, measurements of ozone (O₃) and its precursors were carried out at an urban site in Jinan, a central city in the North China Plain (NCP). A continuous O₃ pollution event was captured during 4–11 August, with the maximum hourly O₃ mixing ratio reaching 154.1 ppbv. Model simulation indicated that local photochemical formation and regional transport contributed 14.0 ± 2.3 and 18.7 ± 4.0 ppbv h⁻¹, respectively, to the increase in O₃ during 09:00–15:00 LT (local time) in this event. For local O₃ formation, the calculated OH reactivities of volatile organic compounds (VOCs) and carbon monoxide (CO) were comparable between O₃ episodes and non-episodes ($p > 0.05$), so was the OH reactivity of nitrogen oxides (NO_x). However, the ratio of OH reactivity of VOCs and CO to that of NO_x increased from 2.0 ± 0.4 s⁻¹ during non-episodes to 3.7 ± 0.7 s⁻¹ during O₃ episodes, which resulted in the change in the O₃ formation mechanism from the VOC-limited regime before the O₃ pollution event to the transitional regime during the event. Correspondingly, the simulated local O₃ production rate during the event (maximum: 21.3 ppbv h⁻¹) was markedly higher than that before the event ($p < 0.05$) (maximum: 16.9 ppbv h⁻¹). Given that

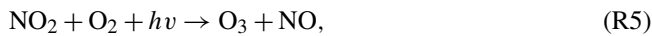
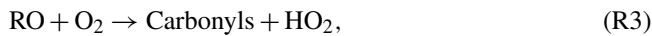
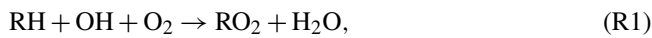
gasoline and diesel exhaust made large contributions to the abundance of O₃ precursors and the O₃ production rate, constraint on vehicular emissions is the most effective strategy to control O₃ pollution in Jinan. The NCP has been confirmed as a source region of tropospheric O₃, where the shift in regimes controlling O₃ formation like the case presented in this study can be expected across the entire region, due to the substantial reductions of NO_x emissions in recent years.

1 Introduction

Air pollution in the North China Plain (NCP), the largest alluvial plain of China consisting of Beijing, Tianjin and many cities in Hebei, Shandong and Henan provinces, has attracted much attention in recent years. While the annual average concentration of PM_{2.5} (particulate matter with aerodynamic diameter less than or equal to 2.5 μm) has been reduced under concerted efforts on emission restrictions (Zhang et al., 2015; Lang et al., 2017), the tropospheric ozone (O₃) pollution, which is less visible than haze but may be equally harmful to human health, is still severe. At a regional receptor site of

the NCP in a mountainous area to the north of Beijing, Wang et al. (2006) reported the maximum hourly O₃ mixing ratio of 286 ppbv. A year-round observation of O₃ at 10 urban sites in Beijing indicated frequent O₃ non-attainments (hourly O₃ > 100 ppbv) through May to August 2013 (Z. Wang et al., 2015). An hourly O₃ mixing ratio of up to 120 ppbv was reported on Mt. Tai, the highest mountain in the NCP (1534 m a.s.l.) (Gao et al., 2005). All these studies revealed the significant photochemical O₃ pollution over the entire NCP. Moreover, O₃ has been increasing in the NCP during the last decades (Zhang et al., 2014, 2015). The increase rate of O₃ at an urban site in Beijing from 2005 to 2011 was quantified as 2.6 ppbv yr⁻¹ (Zhang et al., 2014), comparable to that (1.7–2.1 ppbv yr⁻¹) at Mt. Tai in the summer between 2003 and 2015 (Sun et al., 2016). Overall, the NCP suffers from severe O₃ pollution, which is aggravating.

Apart from the intrusion of stratospheric O₃ in some places with high elevations (Cooper et al., 2005; Lin et al., 2015), photochemical formation is the main source of the ground-level O₃. Volatile organic compounds (VOCs), carbon monoxide (CO) and nitrogen oxides (NO_x) are key precursors of tropospheric O₃ (Crutzen, 1973; Chameides and Walker, 1973; Carter, 1994; Carter et al., 1995). The general chemical Reactions R1–R5 show the production of O₃ from the OH-initiated oxidation of hydrocarbons (RH) (Jenkin et al., 1997; Atkinson, 2000; Jenkin and Clemitshaw, 2000).



The production of O₃ is generally limited by VOCs or NO_x or co-limited by both VOCs and NO_x, depending upon the chemical compositions of the air, particularly the ratio between OH reactivity of VOCs and NO_x (OH reactivity is the sum of the products of O₃ precursor concentrations and the reaction rate constants between O₃ precursors and OH). Xue et al. (2014) indicated that the formation of O₃ was limited by NO_x in Lanzhou in summer, consistent with the findings of Liu et al. (2010), who proved that the NO_x-limited regime dominated O₃ formation in most areas of northwestern China. In southwestern China, O₃ formation was diagnosed as VOC-limited in Chengdu but NO_x-limited in Pengzhou due to the large amount of emissions from petrochemical industry (Tan et al., 2018a). Lyu et al. (2016) reported the VOC-limited regime in Wuhan, a city in central China. The VOC-limited regime has also been repeatedly confirmed for O₃ formation in Shanghai (Xue et al., 2014; Xing et al., 2017) and Nanjing (Ding et al., 2013), eastern China. In the Pearl River Delta of southern China, it was found that O₃ formation was generally limited by VOCs in the southwest, while it was limited by NO_x in the northeast (Ye et al., 2016). In the NCP, both Han et al. (2018) and

Xing et al. (2018) summarized that VOCs limited the production of O₃ in most urban areas. However, in the suburban and rural areas, O₃ formation was generally in the transitional regime, e.g., Yucheng (Zong et al., 2018), or limited by NO_x, e.g., Wangdu (Tan et al., 2018b). From a historical perspective, Jin et al. (2017) pointed out that the sensitivity of O₃ formation to VOCs increased in most Chinese cities but decreased in some megacities (such as Beijing and Shanghai) due to the stringent control of NO_x emissions in recent years. Different VOCs play non-equivalent roles in O₃ formation. Alkenes, aromatics and carbonyls can be readily oxidized by oxidative radicals (e.g., OH) or photolyzed (applicable for carbonyls), leading to O₃ formation (Cheng et al., 2010; Guo et al., 2013). Therefore, the sources with large quantities of emissions of these VOCs generally make considerable contributions to the photochemical production of ground-level O₃. For example, Cheng et al. (2010) pointed out that carbonyls increased the peak O₃ production rates at a rural site and at a suburban site in southern China by 64 % and 47 %, respectively. Solvent-based industry and paint solvent usage with intensive emissions of aromatics were responsible for more than half of the O₃ formation potential in Shanghai (Cai et al., 2010). Carbonyls and alkenes accounted for 71 %–85 % of the total OH reactivity of VOCs in Beijing (Shao et al., 2009).

In addition to the chemical processes, meteorological conditions also play significant roles in the formation, transport and accumulation of O₃. Studies (Chan and Chan, 2000; Huang et al., 2005) indicated that tropical cyclone (typhoon as the mature form) and continental anticyclone are the most common synoptic systems conducive to O₃ pollution in coastal cities of southern China. Many O₃ episodes in eastern China occurred under the control of the Western Pacific Subtropical High (WPSH) (He et al., 2012; Shu et al., 2016). In the NCP (northern China), the summertime O₃ pollution is generally accompanied by weak high-pressure systems (Wang et al., 2010). Furthermore, O₃ pollution is also related to the topography. For example, the mountains to the north and west of Beijing lead to upslope winds (valley breeze) in daytime, which transport the polluted air masses laden with O₃ and/or O₃ precursors from the NCP to Beijing (Lin et al., 2008). Overall, the causes of O₃ pollution are complicated and need to be analyzed case by case.

The NCP is the region with the largest emissions of many air pollutants, such as VOCs and NO_x, in China (Gu et al., 2014; Li et al., 2017), partially accounting for the severe O₃ pollution there. In addition, O₃ pollution in the NCP is closely related to the synoptic systems and topographic features (Chen et al., 2009; Zhang et al., 2016). For example, the strong photochemical production of O₃ in urban plumes of Beijing was found by Wang et al. (2006), while the contribution of regional transport was revealed by the enhanced O₃ production at a rural site in the NCP under southerly winds (Lin et al., 2008). Through the review of synoptic systems in the NCP from 1980 to 2013, Zhang et al. (2016) concluded

that the air quality was generally unhealthy under weak East Asian monsoons. Moreover, a decadal statistical analysis indicated that meteorological factors explained ~ 50 % of the O₃ variations in Beijing (Zhang et al., 2015). Despite many previous studies, the evolutions of the synoptic and photochemical processes in O₃ pollution events and their contributions to the non-attainment of O₃ have been seldom looked into in the NCP. Besides, the local and regional contributions to the elevated O₃ in the NCP are not unambiguously quantified and are limited by the deficiencies in the model representation of either physical or local chemical processes. The situation was even much worse for Jinan, the capital of Shandong province. As early as the 2000s, studies (Shan et al., 2008; Yin et al., 2009) reported the maximum hourly O₃ mixing ratios of 143.8 and 147.8 ppbv in June 2004 and 2005, respectively. Even higher O₃ (198 ppbv) was observed at a rural site downwind of Jinan in June 2013 (Zong et al., 2018). However, almost no study was carried out to explore the mechanisms responsible for high O₃ there, though it has been confirmed that air pollution in the cities like Jinan in the NCP influenced air quality in Beijing (Lin et al., 2008; Wang et al., 2010). To better understand O₃ pollution in the NCP, this study investigated the causes of an O₃ episode event lasting for 8 days in Jinan in summer 2017. The analyses presented here focused on the synoptic systems dominating the Shandong Peninsula during this event, the chemical profiles of O₃ and O₃ precursors, and the simulation of factors contributing to O₃ in Jinan with the aid of a chemical transport model and a photochemical box model. In addition, we proposed feasible O₃ control measures based on the source-resolved OH reactivity of VOCs and NO_x.

2 Methodology

2.1 Site description

The air quality monitoring and sample collection were carried out on the rooftop of a seven-story building on the campus of Shandong University from 15 July to 14 August 2017. The campus is located in the urban area of Jinan, and the site is about 50 m from a main road (Shanda South Road) outside the campus. Figure 1 shows the locations of the sampling site (36.68° N, 117.07° E; 22 m a.g.l.) and the surrounding air quality monitoring stations (AQMSs) set up by the China National Environmental Monitoring Center (CNEMC). Also shown are the observed O₃ and rainfall averaged over 4–11 August 2017 when the O₃ episode event occurred in Jinan. It is noteworthy that the days with maximum hourly O₃ mixing ratios exceeding 100 ppbv (Grade II of National Ambient Air Quality Standard) were defined as O₃ episode days. The hourly O₃ values at the AQMSs were obtained from the website of CNEMC (<http://www.cnemc.cn/>, last access: 12 September 2018). The high O₃ levels at almost all the AQMSs in the NCP (Fig. 1a) indicated a regional O₃ pol-

lution event in this period. In view of the comparable O₃ mixing ratios observed at our sampling site to those at the surrounding AQMSs, we believe that the observations at our sampling site to some extent represented the characteristics of this regional pollution event. This was confirmed by the strong influences of regional transport on O₃ variations at the site, as discussed in Sect. 3.3.

2.2 Air quality monitoring and sample collection

2.2.1 Continuous monitoring of air pollutants and meteorological parameters

O₃, NO and NO₂ were continuously monitored at the sampling site between 15 July and 14 August 2017. The air was drawn through a 4 m Teflon tube by the built-in pumps of the trace gas analyzers at the total flow rate of 2 L min⁻¹ (1.4 L min⁻¹ for O₃ analyzer and 0.6 L min⁻¹ for NO_x analyzer). The inlet was located ~ 1 m above the rooftop of the building. O₃ and NO/NO_x were detected with a UV-based photometric analyzer and a chemiluminescence NO–NO₂–NO_x analyzer, respectively (see Table S1 in the Supplement for the specifications). The lowest NO observed during the sampling period was 2.4 ppbv, which is 6 times the detection limit (DL) of the NO_x analyzer (0.4 ppbv). Since the measurement accuracy of the analyzer was < 15 %, the DL was low enough to not influence the accurate measurements of NO in this study. NO₂ was calculated from the difference between NO and NO_x. Studies indicated that NO₂ monitored with chemiluminescence was generally overestimated due to the conversion of the total odd nitrogen (NO_y) to NO by molybdenum oxide catalysts (McClenny et al., 2002; Dunlea et al., 2007; Xu et al., 2013). The positive bias was more significant in more aged air masses, resulting from higher levels of NO_z (NO_z = NO_y – NO_x) (Dunlea et al., 2007). The average overestimation of NO₂ was 22 % in Mexico City, which even increased to 50 % in the afternoon (Dunlea et al., 2007). Xu et al. (2013) suggested that the chemiluminescence monitors overestimated NO₂ by less than 10 % in urban areas with fresh emission of NO_x, but the positive bias went up to 30 %–50 % at the suburban sites. As described in Sect. 2.1, our sampling site was located in the urban area of Jinan and was only ~ 50 m from a main road. Therefore, we infer that NO₂ might not be significantly overestimated in this study. However, larger overestimation could be expected during O₃ episodes, when the stronger photochemical reactions caused higher production of NO_z. According to Xu et al. (2013), we adopted 30 % (minimum bias in suburban area) and 10 % (maximum bias in urban area) as the maximum fraction of NO₂ overestimation during episodes and non-episodes at this urban site, respectively. The influences of the NO₂ measurement interferences on the results are discussed where necessary.

The hourly concentrations of sulfur dioxide (SO₂) and CO were acquired from a nearest AQMS, which is ~ 1 km from

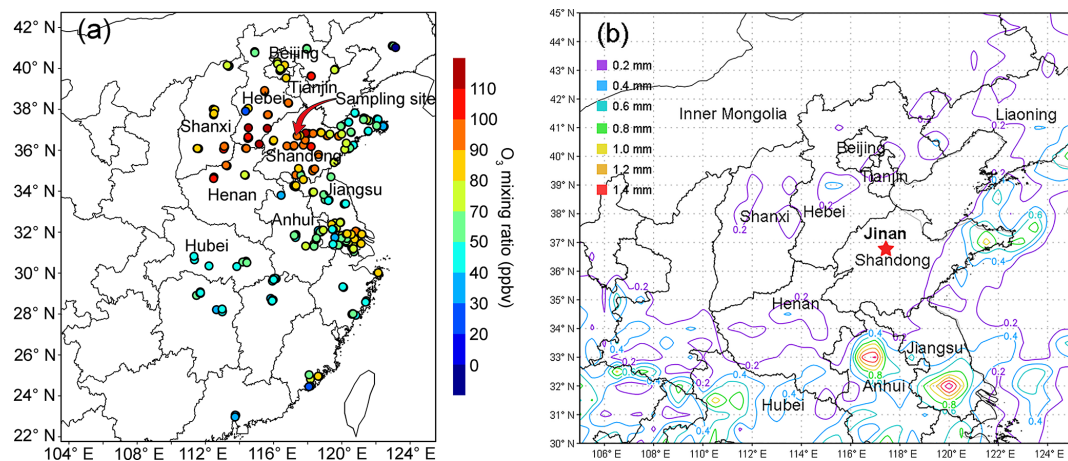


Figure 1. (a) Locations of the sampling site and the CNEMC AQMSs, and the average observed O₃ at 14:00 LT on 4–11 August 2017 (colored circles). The sampling site is overlapped with the nearest AQMS in Jinan. (b) Rainfall distribution, in millimeters (mm), averaged over 4–11 August 2017.

our sampling site. Year-round monitoring of inorganic trace gases was conducted at this AQMS. The air was drawn into the analyzers at a flow of 3 L min⁻¹ through an inlet, ~1 m above the rooftop of a five-story building (~16 m a.g.l.). The specifications of the analyzers deployed at the AQMS are also provided in Table S1. The hourly concentrations of O₃ and NO₂ measured at the AQMS (NO data were not available at the CNEMC website) agreed well with those observed at our sampling site, with the slope of 1.04 ($R^2 = 0.82$) and 1.13 ($R^2 = 0.71$) for O₃ and NO₂ in the linear least squares regressions, respectively (Fig. S1 in the Supplement). Due to the differences in analyzers and/or in sources and sinks of air pollutants between the two sites, the agreements were worse at low mixing ratios for both O₃ and NO₂. Therefore, we only used SO₂ and CO monitored at the AQMS in this study, which had lower photochemical reactivity than O₃ and NO₂ and were more homogeneous at a larger scale.

In addition, the meteorological parameters, including wind speed, wind direction, pressure, temperature and relative humidity, were monitored at the sampling site by a widely used weather station (China Huayun Group, model CAWS600-B). The daily total solar radiation was obtained from the observations at a meteorological station in Jinan (36.6° N, 117.05° E; 170.3 m a.s.l.), 9 km from our sampling site.

2.2.2 Sample collection and chemical analysis

The VOC and oxygenated VOC (OVOC) samples were collected on 9 selective days (i.e., 20 and 30 July and 1, 4–7 and 10–11 August), referred to as VOC sampling days hereafter. The days were selected to cover the periods with relatively high and normal levels of O₃. The high-O₃ days were forecasted prior to sampling based on the numerical simulations of meteorological conditions and air quality. In

total, 6 out of 9 VOC sampling days were O₃ episode days with the maximum hourly O₃ mixing ratio values ranging from 100.4 to 154.1 ppbv. On each day (regardless of episode or non-episode), six VOC and OVOC samples were collected between 08:00 and 18:00 LT every 2 h with the duration of 1 h for VOC and 2 h for OVOC samples. VOC samples were collected with 2 L stainless steel canisters which were cleaned and evacuated before sampling. A flow restrictor was connected to the inlet of the canister to guarantee 1 h sampling. OVOCs were sampled with the 2,4-dinitrophenylhydrazine (DNPH) cartridge, in front of which an O₃ scrubber was interfaced to remove O₃ in the air. A pump was used to draw the air through the DNPH cartridge at a flow of 500 mL min⁻¹. After sampling, all the DNPH cartridges were stored in a refrigerator at 4 °C until chemical analysis.

VOC samples were analyzed using a gas chromatograph with mass selective detector, flame ion detector and electron capture detector system (Colman et al., 2001). In total, 85 VOCs, including 59 hydrocarbons, 19 halocarbons and 7 alkyl nitrates, were quantified. The overall ranges of the DL, accuracy and precision for VOC analysis were 1–154 pptv, 1.2 %–19.8 % and 0.1 %–17.9 %, respectively. The analysis results given by this system have been compared with those analyzed by the University of California, Irvine, and good agreements were achieved (Fig. S2). OVOC samples were eluted with 5 mL acetonitrile, followed by analysis with high-performance liquid chromatography. The DL, accuracy and precision for the detected OVOC species were within the range of 3–11 pptv, 0.32 %–0.98 % and 0.01 %–1.03 %, respectively.

2.3 Model configuration

2.3.1 Chemical transport model

To analyze the processes contributing to high O₃ in Jinan, a chemical transport model, i.e., the Weather Research and Forecasting–Community Multiscale Air Quality (WRF-CMAQ) model, was utilized to simulate O₃ in this study. WRF v3.6.1 was run to provide the offline meteorological field for CMAQ v5.0.2. A two-nested domain was adopted with the resolution of 36 km (outer domain) and 12 km (inner domain). As shown in Fig. S3, the outer domain covered the entire continental area of China, aiming to provide sufficient boundary conditions for the inner domain, which specifically focused on eastern China.

We used the 2012-based Multi-resolution Emission Inventory for China (MEIC) to provide anthropogenic emissions of air pollutants, which was developed by Tsinghua University specifically for China, with the grid resolution of 0.25° × 0.25° (Zhang et al., 2007; He, 2012). Five emission sectors, namely transportation, agriculture, power plant, industry and residence, were included in MEIC. The emission inventory was linearly interpolated to the domains with consideration of the earth curvature effect. For grids outside China, the air pollutant emissions were derived from the INTEX-B (Intercontinental Chemical Transport Experiment Phase B) Asian emission inventory (Zhang et al., 2009). Consistent with many previous studies (Jiang et al., 2010; N. Wang et al., 2015), the Model of Emissions of Gases and Aerosols from Nature (MEGAN) was used to calculate the biogenic emissions. The physical and chemical parameterizations for WRF-CMAQ were generally identical to those described in N. Wang et al. (2015), with the following improvements. Firstly, the carbon bond v5 with updated toluene chemistry (CB05-TU) was chosen as the gas-phase chemical mechanism (Whitten et al., 2010). Secondly, a single-layer urban canopy model (Kusaka and Kimura, 2004) was used to model the urban surface–atmosphere interactions. Thirdly, the default 1990s US Geological Survey data in WRF were replaced by adopting the 2012-based Moderate Resolution Imaging Spectroradiometer (MODIS) land cover data for eastern China. The substitution was performed to update the simulation of boundary meteorological conditions (Wang et al., 2007).

An integrated process rate (IPR) module incorporated in CMAQ was used to analyze the processes influencing the variations of O₃. Through solving the mass continuity equation established between the overall change in O₃ concentration across time and the change in O₃ concentration caused by individual processes, including horizontal diffusion (HDIF), horizontal advection (HADV), vertical diffusion (VDIF), vertical advection (VADV), dry deposition, net effect of chemistry (CHEM) and cloud processes, the O₃ variation rates induced by individual processes were determined. Note that since the estimate of CHEM is influenced

by the estimate of O₃ precursor emissions, the simulation of meteorological conditions and the chemical mechanism, all three aspects should be taken into account wherever CHEM is discussed. The IPR analysis has been widely applied in the diagnosis of processes influencing O₃ pollution (Huang et al., 2005; N. Wang et al., 2015). Since the field observations were conducted near the surface (~ 22 m a.g.l.), and the box model (Sect. 2.3.2) was constrained by the observations, the modeling results on the ground-level layer were extracted from WRF-CMAQ for analyses in this study.

2.3.2 Photochemical box model

We also utilized a photochemical box model incorporating the Master Chemical Mechanism (PBM-MCM) to study the in situ O₃ chemistry, thanks to the detailed (species-based) descriptions of VOC degradations in the MCM (Saunders et al., 2003; Lam et al., 2013). The PBM model was localized to be applicable in Jinan, with the settings of geographic coordinates, sunlight duration and photolysis rates. The photolysis rates were calculated by the TUV (Tropospheric Ultraviolet and Visible) model (Madronich and Flocke, 1997). Specifically, the geographical coordinates, date and time were input into the TUV model to initialize the calculation of solar radiation with the default aerosol optical depth (AOD), cloud optical depth (COD), surface albedo and other parameters. Then, COD was adjusted to make the calculated daily total solar radiation progressively approach the observed value. When the difference between the calculated and observed solar radiation was less than 1 %, the input parameters with the adjusted COD were accepted. Based on the settings, the hourly solar radiations and the photolysis rates of O₃ (J(O¹D)) and NO₂ (JNO₂) were calculated by the TUV model and applied to the PBM-MCM for O₃ chemistry modeling. Table S2 shows the daily maximum J(O¹D) and JNO₂ on the VOC sampling days. The MCM v3.2 (<http://mcm.leeds.ac.uk/MCM/>, last access: 12 September 2018) consists of 17 242 reactions among 5836 species. The mixing ratios of O₃ and its precursors at 00:00 LT on each day were used as the initial conditions for each day's modeling. The initial O₃ therefore represented O₃ left over from the days before the modeling day and partially accounted for the primary OH production. Hourly concentrations of 46 VOCs, 4 OVOCs and 4 trace gases (SO₂, CO, NO and NO₂), as well as hourly meteorological parameters (temperature and relative humidity), were taken as inputs to constrain the model. O₃, as the species to be modeled, was not input except for the setting of initial conditions. The Freon, cycloalkanes and methyl cycloalkanes with low O₃ formation potentials were not included in model inputs either. Also excluded were the species whose concentrations were lower than the DLs in more than 20 % of samples, such as the methyl hexane and methyl heptane isomers. For the hours when measurement data were not available, the concentrations were obtained with linear interpolation. Some secondary species, such as

formaldehyde (HCHO), acetaldehyde and acetone, were input into the model to constrain the simulation. Since other secondary species, e.g., PAN and HNO₃, were not observed in this study, their concentrations were calculated by the model. The model simulated dry depositions of all the chemicals, and the deposition velocities were set identical to those in Lam et al. (2013). Since NO and NO₂ were separately measured, they were not treated as a whole (i.e., NO_x) in the model. Instead, both NO and NO₂ data were input into the model so that the partitioning between them was constrained to observations.

The simulations were separately performed on all the VOC sampling days. For the spin-up, the model was run 72 h prior to the simulation on the day of interest, with the same inputs. The model treated the air pollutants to be well-mixed within the boundary layer, while dilution and transport were not considered. O₃ in the free troposphere was not considered either, due to the lack of O₃ observations above the boundary layer over Jinan. This might hinder the accurate reproduction of the observed O₃, particularly on the days when advection and diffusion were strong. Since the model mainly described the in situ photochemistry, it was validated through comparison with the CHEM process simulated by WRF-CMAQ. The simulated O₃ production rates were output every hour, which were integrated values over every 3600 s in 1 h (model resolution: 1 s). More details about the model configuration can be found in Lam et al. (2013) and Lyu et al. (2017).

3 Results and discussion

3.1 Overall characteristics of O₃ pollution in Jinan

Figure 2 shows the time series of trace gases; OH reactivity of VOCs, CO and NO_x; and meteorological conditions on the VOC sampling days in Jinan (trace gases in the whole sampling period are shown in Fig. S4). All the OH reactivity values discussed in this study were calculated rather than observed ones. The OH reactivity of VOCs was categorized into carbonyls, biogenic VOCs (BVOCs), aromatics, alkenes and alkanes (Table S3 lists the VOCs included in each group). The reaction rate constants between O₃ precursors and OH in the calculation of OH reactivity were adopted from the MCM v3.2. The average total OH reactivity on all the VOC sampling days ($19.4 \pm 2.1 \text{ s}^{-1}$) was comparable to that reported in New York ($19 \pm 3 \text{ s}^{-1}$, Ren et al., 2003), Houston ($9\text{--}22 \text{ s}^{-1}$, Mao et al., 2010) and Beijing ($15\text{--}27 \text{ s}^{-1}$, Williams et al., 2016). Consistent with previous studies in urban areas (Ren et al., 2003; Yang et al., 2016 and references therein), NO_x was the largest contributor ($28.9 \pm 1.9 \%$) to the total OH reactivity. Noticeably, $20.5 \pm 4.1 \%$ of the total OH reactivity was attributable to BVOCs, which were much higher than the contributions in urban areas (< 10 %) reviewed by Yang et al. (2016). The elevated isoprene levels ($2.2 \pm 0.6 \text{ ppbv}$ during episodes and $0.9 \pm 0.3 \text{ ppbv}$ dur-

ing non-episodes) under high temperature (mean: 31°C) explained the considerable contribution of BVOCs to the total OH reactivity in this study.

The total OH reactivity of VOCs and CO (OH reactivity_{VOCs+CO}) was comparable between O₃ episodes ($14.8 \pm 2.0 \text{ s}^{-1}$) and non-episodes ($12.2 \pm 3.0 \text{ s}^{-1}$), so was the OH reactivity of NO_x (4.7 ± 0.8 and $6.9 \pm 1.9 \text{ s}^{-1}$ during episodes and non-episodes, respectively). Taking the positive biases of NO₂ measurements into account (Sect. 2.2.1), we found that the OH reactivity of NO_x was overestimated by up to $17.5 \pm 1.1 \%$ and $5.4 \pm 0.7 \%$ during O₃ episodes and non-episodes, respectively. In the case of maximum overestimation, the actual OH reactivity of NO_x during episodes ($4.0 \pm 0.7 \text{ s}^{-1}$) might be lower ($p < 0.05$) than that during non-episodes ($6.6 \pm 1.9 \text{ s}^{-1}$). The high OH reactivity during non-episodes mainly occurred on 30 July and 1 August, due to the unfavorable meteorological conditions, which are discussed later. Despite the comparable OH reactivity, we found that the ratio of $\frac{\text{OH reactivity}_{\text{VOCs+CO}}}{\text{OH reactivity}_{\text{NO}_x}}$ during O₃ episodes ($3.7 \pm 0.7 \text{ s}^{-1}$) was higher than during non-episodes ($2.0 \pm 0.4 \text{ s}^{-1}$) ($p < 0.05$). The difference was likely even larger, due to the more significant overestimation of NO₂ during episodes. This indicated that O₃ formation was more limited by VOCs during non-episodes than during episodes. Indeed, O₃ formation in Jinan switched from the VOC-limited regime during non-episodes to the transitional regime during episodes (see Sect. 3.4.2). This partially explained the build-up of O₃ on episode days, because the transitional regime features the highest O₃ production rates.

From the aspect of meteorological conditions, O₃ episodes had relatively stronger solar radiation, higher temperature, lower relative humidity and weaker winds ($p < 0.05$). This is reasonable as O₃ formation and accumulation are generally enhanced under these weather conditions. In particular, the solar radiation on 30 July was much weaker than that during O₃ episodes, primarily accounting for the low O₃ on this day. Figure S5 shows the COD retrieved from the Terra MODIS (https://ladsweb.modaps.eosdis.nasa.gov/search/imageViewer/1/MOD06_L2--61/2017-08-06/DB/Site:142/2873994172--3, last access: 12 September 2018) at 10:00–12:00 LT on all the VOC sampling days. The Terra MODIS image revealed thick cloud cover with high COD over Jinan on 30 July, which caused the weak solar radiation. The influences of cloud cover/COD and solar radiation on O₃ pollution are further discussed in Sect. 3.2. Unlike our previous understanding that O₃ pollution is aggravated under high pressure (Chan and Chan, 2000; Zhao et al., 2009), the sea-level pressure during O₃ episodes ($993.4 \pm 0.2 \text{ hPa}$) was significantly lower than during non-episodes ($996.1 \pm 0.4 \text{ hPa}$) in this study ($p < 0.05$). When O₃ reached its hourly maximum on 10 August (154.1 ppbv), the pressure was at its lowest value (990.2 hPa). This discrepancy inspired us to look into the synoptic and chemical processes in this continuous O₃ pollution event.

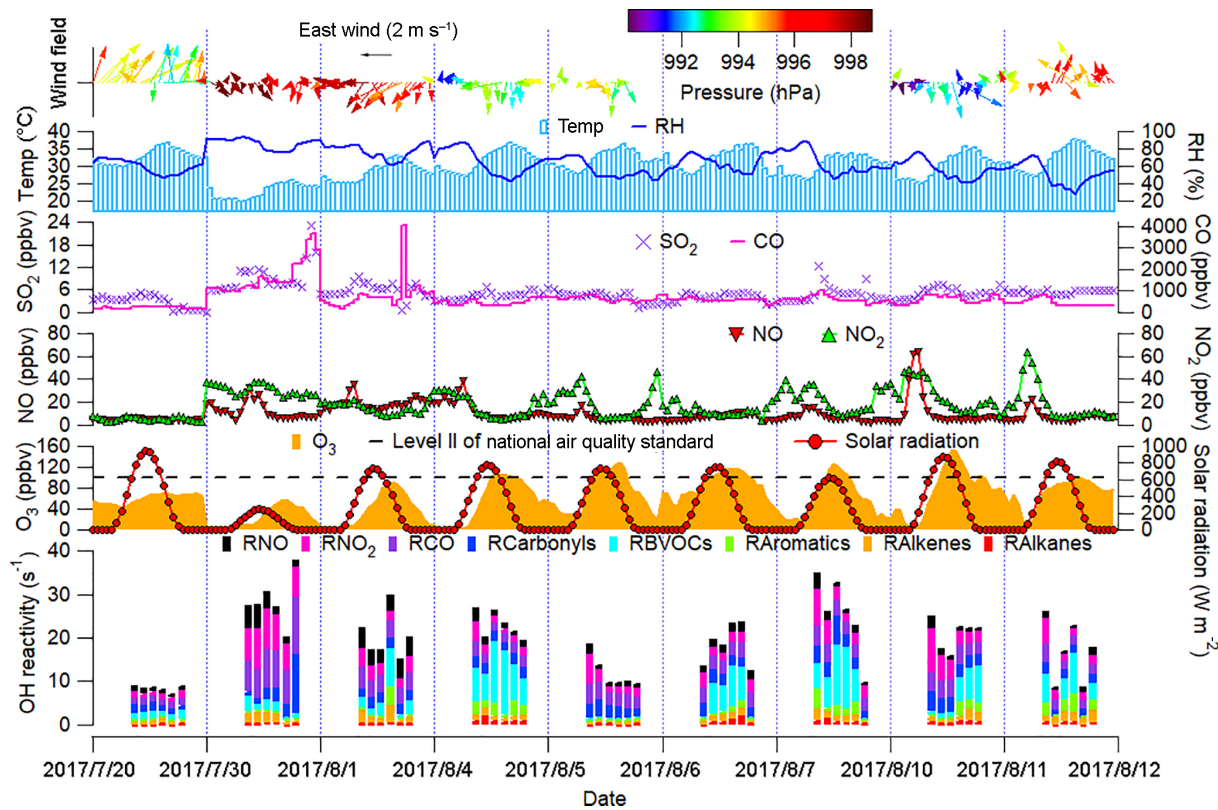


Figure 2. Time series of trace gases, OH reactivity of O₃ precursors and meteorological parameters. Wind speed and wind direction were not monitored from 17:00 LT on 5 August to 23:00 LT on 7 August due to malfunction of the weather station. RH in the top panel denotes the relative humidity. RX in the bottom panel is the OH reactivity of species/group X.

3.2 Synoptic processes and relationship with O₃ pollution

Figure 3 displays the average weather charts at 14:00 LT during O₃ episodes and non-episodes (weather charts on individual VOC sampling days are shown in Fig. S6). Clearly, the temperature in Shandong province was much higher during O₃ episodes than non-episodes, which favored O₃ formation on episode days. Additionally, southerly and southwesterly winds originating from the inland areas (Hubei, Henan and Anhui provinces) prevailed in central and western Shandong during O₃ episodes. In contrast, the winds were generally from the sea or coastal regions in Jiangsu province during non-episodes. It is more likely that O₃ and O₃ precursors were transported to Jinan during episodes. The high concentrations of O₃ precursors on 30 July and 1 August (non-episode days) were mainly caused by the weather conditions (high pressure, low temperature and low solar radiation), as discussed in Sect. 3.1. Further, we also noticed that the winds changed direction from the southwest to the northwest around Jinan during O₃ episodes. This meant that there might be a local circulation, hampering the dispersion of air pollutants during episodes. It seemed that the change in wind direction was caused by the convergence of continental air

and sea breeze from Bohai Bay, similar to the convergence zone formed over the Pearl River estuary in southern China (Fung et al., 2005; Lo et al., 2006). Overall, the surface winds were more favorable for regional transport and accumulation of air pollutants during O₃ episodes. In addition, Shandong province was under the control of a uniform pressure system with the sea-level pressure of 1000–1001 hPa during O₃ episodes, implying the relatively stagnant weather.

To better understand the relationship between O₃ pollution and the synoptic systems, Table 1 summarizes the synoptic systems, weather conditions and air mass origins on all the VOC sampling days. The weather charts at surface level and 500 hPa on 1, 4, 7, 10 and 13 August are presented in Figs. S7 and S8, showing the evolution of the synoptic systems. To identify the origins of air masses, the backward trajectories of air masses are shown in Fig. 4. The trajectories were computed using the Hybrid Single-Particle Lagrangian Integrated Trajectory (HYSPLIT) model v4.9. Each trajectory was calculated for 48 h and the calculation was done every 6 h (four trajectories each day). Our sampling site (36.68° N, 117.07° E) was set as the end point of the trajectories with the height of 500 m a.s.l. The discrepancy between the wind direction and origin of air masses, e.g., on 1 and 11 August, was likely due to the air recirculation at the ground level.

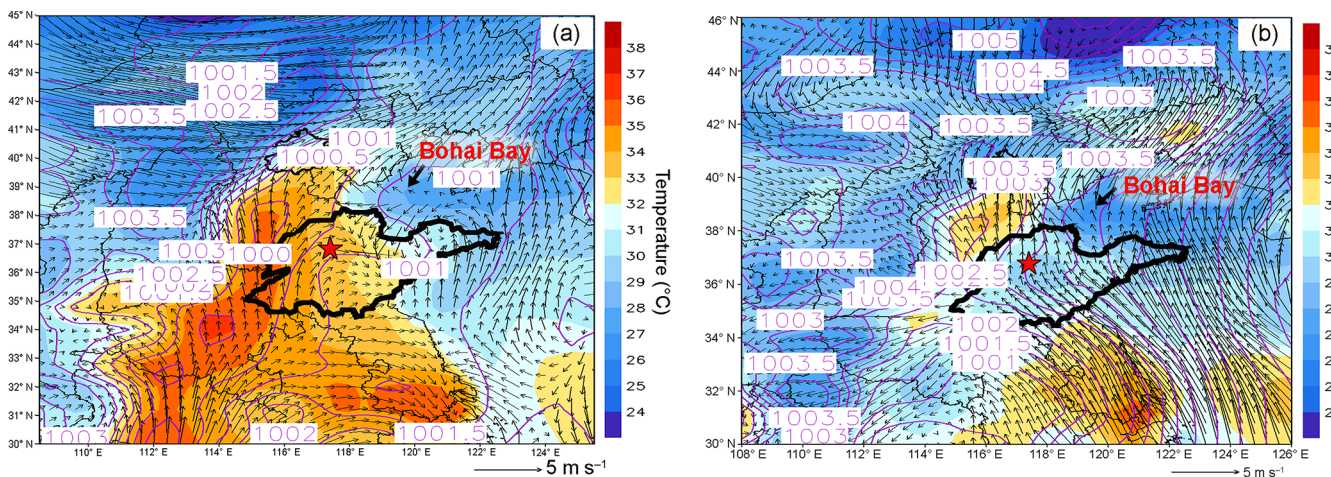


Figure 3. Weather chart at 14:00 LT averaged over (a) O₃ episodes and (b) non-episodes. The red star represents Jinan. The dark black line is the boundary of Shandong province. Bohai Bay is located to the northeast of Shandong province. Numbers in the figure are sea-level pressures in units of hectopascal (hPa).

It was found that Jinan was under the control of the WPSH on 20 July (weather chart on 500 hPa is not shown here), and the air masses arriving in Jinan originated from southern China (Fig. 4). As anticipated, the WPSH caused high temperatures and the intensive solar radiation (Fig. 2), which was conducive to O₃ formation. However, the winds on 20 July were the strongest in the entire VOC sampling period, with the highest hourly wind speed of 3.9 m s⁻¹. The strong winds facilitated the dispersion of O₃ and its precursors, leading to low O₃ levels on this day. The WPSH moved southward on the following days and Jinan was controlled by a uniform pressure system, which was formed in the peripheries of two low-pressure systems (two rain belts as shown in Fig. 1), i.e., one over central China and another over northern China (Fig. S7). Thus, the pressure in Jinan was relatively high (997.1 ± 0.3 hPa), compared to the south and north regions. This synoptic system lasted for several days until 7 August, covering 2 non-episode days and 4 O₃ episode days. The low O₃ on 2 non-episode days (30 July and 1 August) was mainly attributable to the weak solar radiation and low temperature as discussed above.

In contrast, continuously strong solar radiations with low COD (Figs. 2 and S5), high temperature and continental air masses (Fig. 4) were observed on 4–7 August. This, in addition to the shift in the O₃ formation mechanism (see Sects. 3.1 and 3.4.2), explained the prolonged O₃ pollution event. On 10 August, the rain belt over northern China moved southward, forming a deep low-pressure trough over the NCP, and Jinan was behind the trough (Fig. S8d). The low-pressure trough is a typical synoptic system conducive to O₃ pollution, resulting from the intrusion of O₃ in the stratosphere and/or the upper troposphere (Chan and Chan, 2000). Moreover, there was nearly no cloud cover over the entire NCP on 10 August (Fig. S5). Consequently, the high-

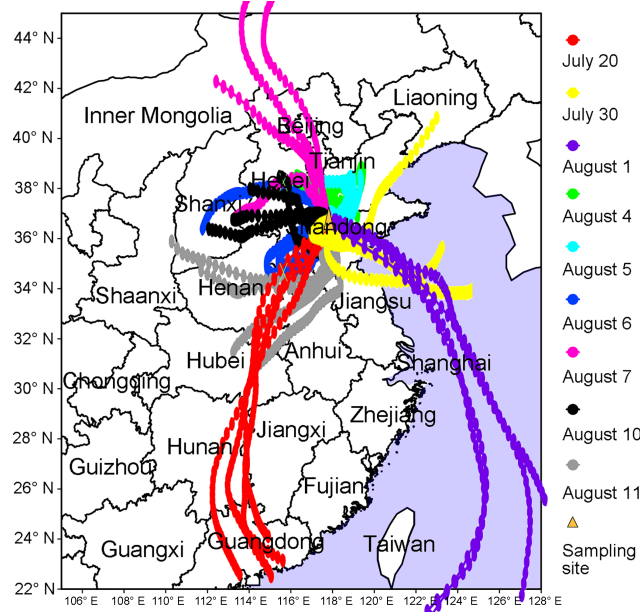


Figure 4. The 48 h backward trajectories calculated every 6 h, with Jinan (36.68° N, 117.07° E; 500 m a.g.l.) as the ending point. The trajectories are simulated by HYSPLIT v4.9. The water areas are highlighted in blue.

est O₃ (154.1 ppbv) in this sampling campaign was observed. On 11 August, the low-pressure system continued to extend to the Yellow Sea. O₃ decreased substantially on this day with the disappearance of the low-pressure trough and the weakening of solar radiation, though the hourly maximum O₃ mixing ratio still reached 100.4 ppbv. On the following days, the precipitations relieved the O₃ pollution in Jinan.

Table 1. Summary of the synoptic systems, weather conditions and air mass origins on VOC sampling days.

| Date | Maximum hourly O ₃ (ppbv) | Episode/non-episode | Synoptic system weather condition | Air mass origin |
|-----------|--------------------------------------|---------------------|--|---|
| 20 July | 71.0 | Non-episode | WPSH, strong southwesterly winds | Continental air masses from southern China |
| 30 July | 57.6 | | Uniform pressure field (weak high pressure), rain, fog, calm winds | |
| 1 August | 90.6 | | Uniform pressure field (weak high pressure), northeasterly winds | Marine air masses |
| 4 August | 107.5 | | Uniform pressure field (weak high pressure), northeasterly winds | |
| 5 August | 128.2 | | Uniform pressure field (weak high pressure), calm winds | Continental air masses from Shandong province |
| 6 August | 116.9 | Episode | Uniform pressure field (weak high pressure), southwesterly winds | |
| 7 August | 126.9 | | Uniform pressure field (weak high pressure), calm winds | Continental air masses from the north |
| 10 August | 154.1 | | Low-pressure trough, calm winds | Continental air masses from the west |
| 11 August | 100.4 | | Subtropical high, southeasterly winds | Continental air masses from the southwest |

3.3 O₃ simulation and process analysis

The observations indicated the likely different regimes controlling local O₃ formation and the potential impacts of regional transport. To understand the atmospheric chemistry and dynamics, as well as their roles in this O₃ pollution event, the WRF-CMAQ was applied. Figure 5 shows the hourly average simulated and observed O₃ on the VOC sampling days in Jinan. Overall, the model reproduced the magnitudes and diurnal patterns of the observed O₃ well, except for the higher simulated O₃ on 20 July and the under-prediction of O₃ on 1, 7 and 10 August. Discussions on the discrepancies and the model validation were provided in Text S1, Figs. S9–S11 and Table S4.

The IPR analysis quantified the O₃ variation rates induced by different processes, as shown in Fig. 6. HDIF and HADV were summed as horizontal transport (HTRA), and the vertical transport (VTRA) was a total representative of VDIF and VADV. It was found that chemical reactions generally led to the decrease in the O₃ mixing ratio during non-episodes. The negative contributions of chemical reactions on 20 July coincided with the very low concentrations of O₃ precursors and

the flat diurnal cycle of O₃ (Fig. 2). The chemical destruction to O₃ on 30 July and 1 August was most likely related to the weak solar radiation and low temperature, which inhibited the photochemical reactions. In fact, the negative chemical effect should be considered as the titration of NO to the regionally transported and/or background O₃ and the depletion of O₃ by the freshly emitted NO near the sources (Beck and Grennfelt, 1994; Sillman, 1999). Conversely, the combined effect of horizontal and vertical transport was to increase O₃ levels during non-episodes.

During O₃ episodes, chemical reactions made positive contributions to O₃ production rates between 09:00 and 15:00 LT, with the average hourly O₃ production rate of $14.0 \pm 2.3 \text{ ppbv h}^{-1}$. At the same time, O₃ was also elevated by transport at an average rate of $18.7 \pm 4.0 \text{ ppbv h}^{-1}$, as a combined effect of vertical transport ($-40.8 \pm 20.2 \text{ ppbv h}^{-1}$) and horizontal transport ($59.5 \pm 19.8 \text{ ppbv h}^{-1}$). The negative contribution of vertical transport to O₃ in these hours might be caused by the updraft with the increase in temperature in the city. The positive contributions of horizontal transport could be explained by the air masses laden with O₃ originating from the west and the north (Figs. 4 and S10). The much-

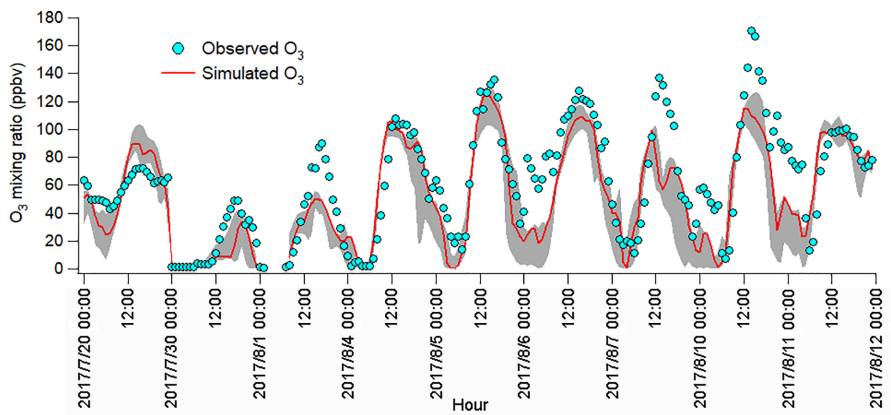


Figure 5. Hourly average mixing ratios of the WRF-CMAQ simulated and observed O₃ in Jinan. The grey area shows the minimum and maximum simulated O₃ at the sampling site and eight adjoining grids (12 km × 12 km for each grid).

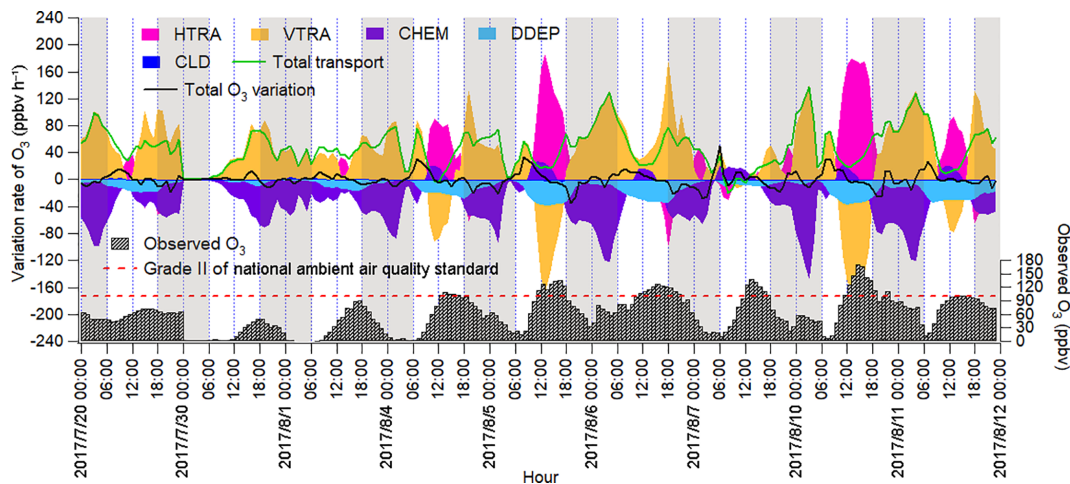


Figure 6. Time series of O₃ variation rate in Jinan induced by individual processes calculated based on the change in O₃ per hour. Total transport is the sum of HTRA and VTRA, and the sum of O₃ variation rates attributable to all the processes is represented by the total O₃ variation rate. The nighttime (18:00–06:00 LT) has been highlighted in grey.

higher O₃ over the NCP than in the surrounding regions indicated that the NCP was an O₃ source in this case. In fact, the transport of O₃ from the lower troposphere over the NCP to the free troposphere and further to northeast China was also presented by Ding et al. (2009).

During 16:00–08:00 LT on O₃ episode days, O₃ was titrated and chemically consumed at the rate of $49.4 \pm 6.3 \text{ ppbv h}^{-1}$. This was reasonable, because the fresh vehicular emissions in the morning and evening rush hours consumed O₃, particularly the irreversible titration of NO to O₃ in the absence of sunlight. The NO₂ produced from the titration reaction was carried over to the other places by air circulation and/or oxidized to NO₃ and N₂O₅, which could further react with aerosol to form HNO₃ and CINO₂ in the evening. Horizontal and vertical transport dominated O₃ sources, with the average positive contribution of 5.7 ± 7.0 and $54.5 \pm 9.6 \text{ ppbv h}^{-1}$ during 16:00–08:00 LT on 4–11 August, re-

spectively. The strong vertical transport coincided with the downward winds in the evening, which brought the high-altitude O₃ to the ground, as indicated in Fig. S9. However, the sources of O₃ in the upper atmosphere were beyond the scope of this study.

3.4 Local O₃ formation and control

3.4.1 Pathway and source contributions to O₃ production

The IPR analyses showed that chemical reactions served as an important source of O₃ on episode days in Jinan, particularly during 09:00–15:00 LT when O₃ was at high levels. This process was further studied through the simulation of the in situ photochemistry by PBM-MCM. It should be noted that the simulations were based on the observed concentrations of O₃ precursors, which could be influenced by

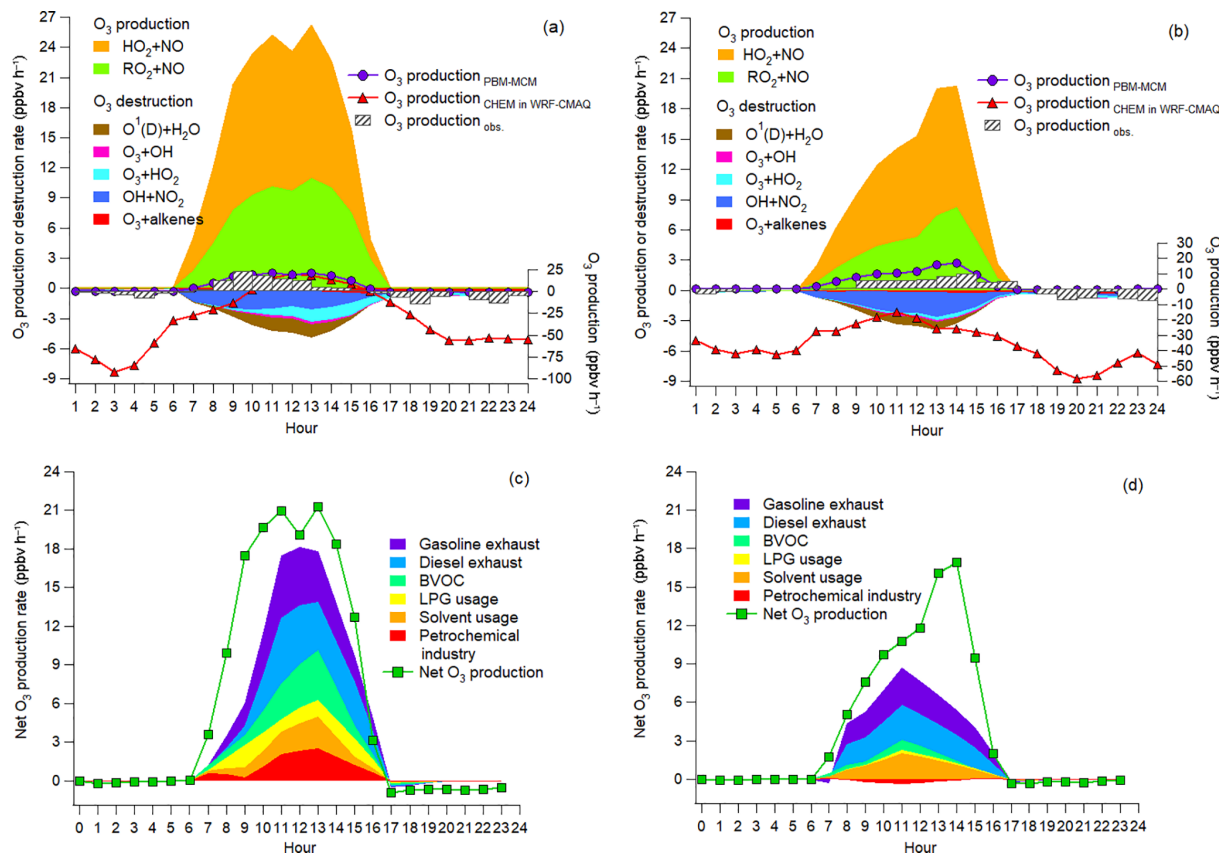


Figure 7. Pathway contributions to O₃ production and destruction rate during episodes (a) and non-episodes (b). Contributions of O₃ precursor sources to the net O₃ production rate during episodes (c) and non-episodes (d).

both local and regional air. Caution was required to extend the results to all the situations in Jinan, because the regional effect was not always consistent. Table S5 lists the production and destruction pathways of O₃ (Thornton et al., 2002; Monks, 2005; Kanaya et al., 2009). Briefly, the oxidation of NO by HO₂ and RO₂ produced NO₂, which led to O₃ formation following NO₂ photolysis (Reactions R2 and R4–R5 in Sect. 1). Therefore, the reactions between NO and HO₂/RO₂ were considered as the production pathways of O₃. To account for O₃ destruction, the reaction between O^{1(D)} and H₂O denoted the photolysis of O₃, and reactions of O₃ with OH, HO₂ and alkenes were also included. Furthermore, since HNO₃ was an important sink of NO₂, the reaction between OH and NO₂ was treated to be destructive to O₃. The titration of O₃ by NO was not included in O₃ destruction, because NO₂ produced in this reaction was not considered as a source of O₃.

Figure 7a and b show the average diurnal cycles of the simulated contributions to O₃ production rates of different pathways. Also shown are the net O₃ production rates simulated by PBM-MCM (O₃ production_{PBM-MCM}), those simulated by WRF-CMAQ (O₃ production_{CHEM}) and those calculated from the observed hourly O₃ (O₃ production_{obs.}). Overall, O₃

production_{PBM-MCM} and O₃ production_{obs.} were on the same magnitudes, especially during O₃ episodes with more stagnant weather conditions. This indicated that the PBM-MCM model reasonably reproduced the in situ O₃ photochemistry. Though obvious discrepancies existed between O₃ production_{CHEM} and O₃ production_{PBM-MCM}, they agreed well with each other during 10:00–15:00 LT on episode days, consistent with the finding that chemical reactions made great contributions to O₃ in these hours (Fig. 6). The lower or even negative O₃ production_{CHEM} resulted from the titration of the regionally transported and/or local background O₃ by NO and the following depletion of NO₂ through reaction with OH and/or dispersion. Differently, PBM-MCM did not consider the transport of O₃, though the transport effect was partially represented by constraining the model to the observed concentrations of O₃ precursors. In addition, the PBM-MCM was constructed by the observed air pollutants, which were already subject to chemical reactions before being detected by the analytical instruments. This meant that the reaction between NO and O₃ from the emission to the detection of NO_x was not considered in PBM-MCM. However, as an emission-based model, WRF-CMAQ performed better in describing the reactions immediately after the emissions

Table 2. Contributions to VOCs, CO, NO, NO₂ and the O₃ production rate by the sources of O₃ precursors averaged on the VOC sampling days in Jinan (Unit: % unless otherwise specified).

| Source | VOCs* | CO | NO | NO ₂ | O ₃ production rate (ppbv h ⁻¹) | |
|----------------------|------------|------------|------------|-----------------|--|--------------|
| | | | | | O ₃ episodes | Non-episodes |
| GE ¹ | 25.7 ± 3.6 | 29.9 ± 2.1 | 30.9 ± 2.4 | 22.2 ± 2.4 | 1.8 ± 0.6 | 1.0 ± 0.3 |
| DE ² | 17.6 ± 2.4 | 57.3 ± 5.2 | 52.0 ± 5.8 | 54.4 ± 5.8 | 1.7 ± 0.4 | 1.0 ± 0.3 |
| BVOC | 6.1 ± 2.6 | 0.0 ± 1.7 | 0.0 ± 2.8 | 0.0 ± 2.3 | 1.2 ± 0.5 | 0.2 ± 0.1 |
| LPG ³ | 14.7 ± 2.0 | 2.2 ± 1.1 | 9.1 ± 1.6 | 4.7 ± 0.9 | 0.8 ± 0.5 | 0.1 ± 0.1 |
| Solvent ⁴ | 17.1 ± 3.9 | 3.1 ± 1.8 | 5.1 ± 3.8 | 7.8 ± 3.1 | 0.8 ± 0.5 | 0.7 ± 0.3 |
| PI ⁵ | 18.8 ± 3.1 | 7.4 ± 1.9 | 2.9 ± 1.8 | 10.9 ± 2.5 | 1.0 ± 0.3 | -0.1 ± 0.1 |

VOCs*: VOCs applied in source apportionment (see Text S2). ¹ Gasoline exhaust. ² Diesel exhaust. ³ Liquefied petroleum gas (LPG) usage. ⁴ Solvent usage. ⁵ Petrochemical industry.

of air pollutants. Therefore, the chemical destruction of O₃ in the vicinity of NO_x sources also accounted for the aforementioned discrepancy. The obviously higher reaction rates between NO and O₃ simulated by WRF-CMAQ (Fig. S12) confirmed our inferences.

During both O₃ episodes and non-episodes, the reaction between HO₂ and NO dominated over RO₂ + NO in O₃ production, while the O₃ destruction was mainly attributable to the formation of HNO₃, the reaction between O₃ and HO₂, and photolysis of O₃. The net O₃ production rate during O₃ episodes (maximum: 21.3 ppbv h⁻¹) was much ($p < 0.05$) higher than during non-episodes (maximum: 16.9 ppbv h⁻¹), which partially explained the higher O₃ on episode days. In general, OH + NO₂ serves as the chain-terminating reaction in the VOC-limited regime of O₃ formation, while the radical–radical reactions take over the role in the NO_x-limited regime (Finlayson-Pitts and Pitts Jr., 1993; Kleinman, 2005). Here, we found that the ratio of total reaction rates between HO₂ + RO₂ and OH + NO₂ substantially increased from 0.2 ± 0.1 during non-episodes to 1.0 ± 0.3 during O₃ episodes ($p < 0.05$). This suggested that O₃ formation during non-episodes was limited by VOCs, while it switched to being co-limited by VOCs and NO_x during O₃ episodes in view of the equivalent role of HO₂ + RO₂ and OH + NO₂ in terminating the chain reactions.

Further, the contributions to the net O₃ production rates of different sources of O₃ precursors were identified, as presented in Fig. 7c and d. Text S2 and Fig. S13 illustrate the source apportionment of O₃ precursors and the simulations of the source-specific contributions to O₃ production rates. The results are presented in Table 2. Since the source apportionment was performed for the ambient O₃ precursors which were already subject to atmospheric processes, such as dispersion, deposition and chemical reactions, the results represented the source contributions to the steady-state concentrations of O₃ precursors and the corresponding O₃ production rates. It was found that gasoline exhaust and diesel exhaust were the largest contributors to O₃ production rates regard-

less of O₃ episodes or non-episodes. Further, the net O₃ production rates attributable to gasoline exhaust (diesel exhaust) increased from 1.0 ± 0.3 ppbv h⁻¹ (1.0 ± 0.3 ppbv h⁻¹) during non-episodes to 1.8 ± 0.6 ppbv h⁻¹ (1.7 ± 0.4 ppbv h⁻¹) during O₃ episodes. This suggested that vehicular emissions played critical roles in building up ground-level O₃ in the O₃ pollution event. If carbonyls were taken into account, the contributions of vehicular emissions to O₃ production rates were even higher than the currently simulated values, due to the abundances of carbonyls in vehicle exhausts (Grosjean et al., 1990; Granby et al., 1997). In addition, the contributions of the other sources to O₃ production rates all increased during O₃ episodes except for solvent usage ($p > 0.05$), as listed in Table 2. It is not surprising to see the synchronous increases, because of the stronger solar radiation and higher temperature during episodes.

Further insight into the percentage contributions (not shown here) found that the contributions of BVOC, liquefied petroleum gas (LPG) usage and petrochemical industry to O₃ production rates increased substantially from 9.9 ± 4.2 %, 4.3 ± 1.4 % and -2.8 ± 1.9 % during non-episodes to 19.2 ± 4.3 %, 9.1 ± 3.4 % and 12.1 ± 3.1 % during O₃ episodes, respectively. The increased O₃ production rates by BVOCs could be explained by the increase in isoprene (episodes: 2.2 ± 0.6 ppbv; non-episodes: 0.9 ± 0.3 ppbv) under higher temperature and stronger solar radiation during O₃ episodes. The enhancement of O₃ production rates driven by petrochemical industry on episode days was likely associated with the dominance of continental air (Fig. 4) and the extensive petrochemical industries in the NCP. For example, the mixing ratio of styrene increased from 54.7 ± 22.0 pptv during non-episodes to 162.3 ± 44.7 pptv during O₃ episodes. The reason for elevated O₃ production rates resulting from LPG usage during episodes was unknown. It is worth noting that the source contributions to O₃ production rates might have some uncertainties due to the limited number of samples (54 samples) and O₃ precursors (31 VOCs, CO, NO and NO₂) applied for source apportionment.

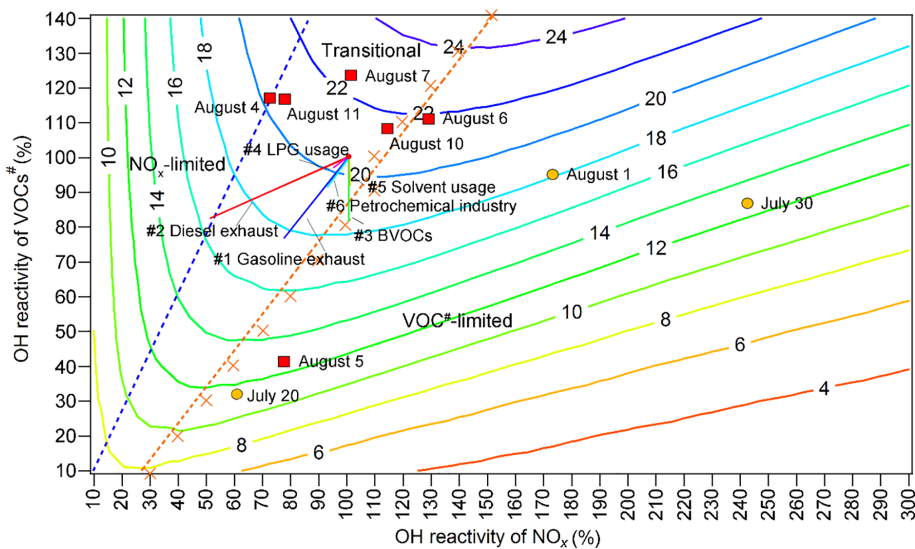


Figure 8. Isopleths of the net O₃ production rate (ppbv h⁻¹) at 12:00 LT as a function of OH reactivity_{VOCs[#]} and OH reactivity_{NO_x}. The red blocks and orange circles denote the calculated OH reactivity_{VOCs[#]} and OH reactivity_{NO_x} values at 12:00 LT on O₃ episode and non-episode days, respectively. Each orange cross represents the OH reactivity_{VOCs[#]} and OH reactivity_{NO_x} at 12:00 LT in the scenario with the highest O₃ production rate at a given OH reactivity_{VOCs[#]}. The dashed orange line and dashed blue line divide O₃ formation into the VOC-limited regime, transitional regime and NO_x-limited regime. Line 1 (solid straight blue line): gasoline exhaust; line 2 (straight red line): diesel exhaust; line 3 (straight green line): BVOCs; line 4 (straight pink line): LPG usage; line 5 (solid straight orange line): solvent usage; line 6 (straight light-blue line): petrochemical industry.

3.4.2 O₃ control measures

Both WRF-CMAQ and PBM-MCM revealed the significant local O₃ formation in the O₃ pollution event. The relationships between O₃ and its precursors needed to be clarified so that the science-based control measures could be taken. Throughout the VOC sampling period, the OH reactivity values of VOCs (OH reactivity_{VOCs}) were within the range of 33 %–123 % of the average OH reactivity_{VOCs} during O₃ episodes. For OH reactivity of NO_x (OH reactivity_{NO_x}), the range was 61 %–242 %. The O₃ production rates were simulated in a set of assumed scenarios with different OH reactivity_{VOCs} and OH reactivity_{NO_x} values. To include the OH reactivity of VOCs and NO_x on all the VOC sampling days, factors from 10 % to 140 % with the step of 10 % were applied to the average diurnal profiles of VOCs and CO during O₃ episodes, while the factors ranged from 10 % to 300 % with the step of 10 % for NO_x. The initial concentrations of all the air pollutants were also scaled by the factors, and the model was constrained to these scaled concentrations every hour, except for O₃. It should be noted that the factors applied to CO were exactly the same as those applied to VOCs; therefore we use VOCs[#] to represent the sum of VOCs and CO hereafter. The 14 gradients of OH reactivity_{VOCs[#]} values and 30 gradients of OH reactivity_{NO_x} values made up 420 scenarios. Meteorological conditions were exactly the same for all the scenarios and the clear sky was hypothesized. According to the simulations, the maximum O₃ production

rates occurred at 12:00 LT. Thus, the simulated O₃ production rates at 12:00 LT, as a function of percentages of OH reactivity_{VOCs} and OH reactivity_{NO_x}, are plotted in Fig. 8.

Text S3 describes the methods to define the regimes of O₃ formation. Overall, O₃ formation was mainly limited by VOCs[#] during non-episodes. However, it switched to being co-limited by VOCs[#] and NO_x (transitional regime) on episode days with the net O₃ production rates being among the highest, except for 5 August when the strong sea breeze diluted air pollutants in Jinan and/or intercepted the transport of air pollutants from central China to Jinan (Fig. S6). In fact, the sensitivity of O₃ formation to NO_x might be underemphasized due to the positive biases of NO₂ measurements (Lu et al., 2010). This effect was expected to be more significant during episodes when the overestimation of NO₂ was more obvious. However, O₃ formation was not likely only limited by NO_x even during O₃ episodes because NO₂ could not be overestimated by more than 30 % according to our inferences (see Sect. 2.2.1). Therefore, O₃ formation was treated to be in the transitional regime during episodes. This partially explained the increased O₃ during episodes in Jinan, given the higher O₃ production rates in the transitional regime (Fig. 8). Noticeably, the change in regimes controlling O₃ formation is consistent with that predicted by the $\frac{\text{OH reactivity}_{\text{VOCs}^{\#}}}{\text{OH reactivity}_{\text{NO}_x}}$ ratio and the ratio of the reaction rates between HO₂ + RO₂ and OH + NO₂.

The source apportionment of O₃ precursors enabled us to calculate the source-specific OH reactivity_{VOCs[#]} and OH

reactivity_{NO_x} values. Accordingly, the variations in O₃ production rates induced by the reductions in source emissions are presented in Fig. 8 (straight solid lines 1–6). The start point of the straight lines corresponded to 100% of the total average OH reactivity_{VOCs*} and OH reactivity_{NO_x} during O₃ episodes. The end points, however, represented the OH reactivity_{VOCs*} and OH reactivity_{NO_x} with the complete removal of emissions from the individual sources. Therefore, the differences of the O₃ production rates between the start point and end points were the source contributions to the O₃ production rates, while the lengths of the lines reflected the contributions to the OH reactivity of the sources. Further, the simulated O₃ production rates on the lines 1–6, as a response of reductions in source emissions, are extracted and plotted in Fig. S14. Obviously, the highest efficiencies of O₃ reduction could be achieved by cutting diesel exhaust (0.58 ppbv h⁻¹/10 % emission reduction) and gasoline exhaust (0.47 ppbv h⁻¹/10 % emission reduction). In fact, the sensitivities of O₃ production rates to the vehicle exhausts might be somewhat underestimated, due to the exclusion of carbonyls in the source apportionment. However, the reductions of O₃ production rates by cutting 10 % of vehicle exhausts were still insignificant, compared to the overall maximum O₃ production rate of 21.3 ppbv h⁻¹ during O₃ episodes. This indicated that, by only restraining emissions from one to two sources, high percentages of emission reductions were required to sufficiently reduce the overall O₃ production rate. Otherwise, a combined effort should be made to control the emissions of O₃ precursors from the diverse sources. In particular, it is essential to get rid of the transitional regime featuring high O₃ production rates.

4 Implications

This study investigates the causes of a severe O₃ pollution event lasting for 8 consecutive days in the NCP, one of the most densely populated regions in the world. Photochemical formation in the lower troposphere of the NCP is demonstrated as the main source of O₃, under the control of weak high-pressure or low-pressure trough. Though the emissions of NO_x, an important precursor of O₃, have been significantly reduced in China since 2013 (Duncan et al., 2016; Liu et al., 2017), O₃ pollution is still severe or even worsening in the NCP, as revealed in the present and also previous studies (Zhang et al., 2014; Sun et al., 2016). The finding that O₃ formation shifted from the VOC-limited regime on relatively low O₃ days to the transitional regime on O₃ non-attainment days may elucidate the increase in O₃, because O₃ production rates in the transitional regime are the highest. It is unrealistic to expect the continuously linear reduction in NO_x emissions in the NCP after the substantial decreases in emissions from power plants and industries in recent years. In other words, restraining VOC emissions is urgent for O₃ abatement in the NCP. Another important finding

in this study is that the NCP served as an O₃ source. This was proposed by Ding et al. (2009), based on the aircraft measurement and simulation of atmospheric dynamics. We confirm it through the ground-level observation and the simulation of in situ photochemistry. It can be expected that organic nitrates are also intensively formed in the NCP as byproducts of O₃ formation. In view of the fact that the NCP is located within the midlatitude band of Northern Hemisphere under the dominance of westerlies, we believe that O₃ and organic nitrates formed in this region may be transported over a long distance following the uplifting of air masses, which has been confirmed to partially account for the enhancement of background O₃ in North America and even Europe (Deren et al., 2015; Lin et al., 2017). Therefore, the recent air pollution control measures taken in China (including China's Clean Air Action Plan in force in 2013) (Zheng et al., 2018) are still inadequate to ease the burden of global tropospheric O₃ in a short period. More effective action plans should be implemented for O₃ abatement, with comprehensive thinking of atmospheric dynamics and chemistry.

Data availability. The data are accessible at https://drive.google.com/open?id=1_KeOxOuVsLY83xL74RtcRORsiyIR8FZ (Lyu, 2018).

Supplement. The supplement related to this article is available online at: <https://doi.org/10.5194/acp-19-3025-2019-supplement>.

Author contributions. The study was designed by the corresponding author, HG, with the help of LH and YZ. FJ and HC provided valuable input on the characteristics of meteorological conditions and emissions of air pollutants in the NCP. XL collected the samples and managed the logistics in the field campaign, and LX provided sufficient assistance in field sampling campaign. The solar radiation data in Jinan were obtained from ZC. XL performed data analyses and wrote the paper, while the chemical transport modeling was done by NW and YZ. HG revised and finalized the paper for submission.

Acknowledgements. This study was supported by the National Key R & D Program of China (2017YFC0212001); the Research Grants Council of the Hong Kong Special Administrative Region via grants PolyU5154/13E, PolyU52052/14E, PolyU52052/16E, CRF/C5004-15E and CRF/C5022-14G; the Collaborative Research program between the Beijing University of Technology and the Hong Kong Polytechnic University (PolyU) (4-ZZFW); the Hong Kong Polytechnic University PhD scholarships (project RTUP); and the National Natural Science Foundation of China (no. 41675118). This study was partly supported by the Hong Kong PolyU internal grant (G-YBUQ, 1-ZVJT and 1-BBW4). The valuable comments of the anonymous reviewers were highly appreciated.

Edited by: Steven Brown

Reviewed by: two anonymous referees

References

- Atkinson, R.: Atmospheric chemistry of VOCs and NO_x, *Atmos. Environ.*, 34, 2063–2101, 2000.
- Beck, J. P. and Grennfelt, P.: Estimate of ozone production and destruction over northwestern Europe, *Atmos. Environ.*, 28, 129–140, 1994.
- Cai, C., Geng, F., Tie, X., Yu, Q., and An, J.: Characteristics and source apportionment of VOCs measured in Shanghai, China, *Atmos. Environ.*, 44, 5005–5014, 2010.
- Carter, W. P.: Development of ozone reactivity scales for volatile organic compounds, *Air Waste Manage. Assoc.*, 44, 881–899, 1994.
- Carter, W. P., Pierce, J. A., Luo, D., and Malkina, I. L.: Environmental chamber study of maximum incremental reactivities of volatile organic compounds, *Atmos. Environ.*, 29, 2499–2511, 1995.
- Chameides, W. and Walker, J. C.: A photochemical theory of tropospheric ozone, *J. Geophys. Res.*, 78, 8751–8760, 1973.
- Chan, C. Y. and Chan, L. Y.: Effect of meteorology and air pollutant transport on ozone episodes at a subtropical coastal Asian city, Hong Kong, *J. Geophys. Res.-Atmos.*, 105, 20707–20724, 2000.
- Chen, Y., Zhao, C., Zhang, Q., Deng, Z., Huang, M., and Ma, X.: Aircraft study of mountain chimney effect of Beijing, China, *J. Geophys. Res.-Atmos.*, 114, D08306, <https://doi.org/10.1029/2008JD010610>, 2009.
- Cheng, H., Guo, H., Wang, X., Saunders, S. M., Lam, S. H. M., Jiang, F., Wang, T., Ding, A., Lee, S., and Ho, K. F.: On the relationship between ozone and its precursors in the Pearl River Delta: application of an observation-based model (OBM), *Environ. Sci. Pollut. Res.*, 17, 547–560, 2010.
- Colman, J. J., Swanson, A. L., Meinardi, S., Sive, B. C., Blake, D. R., and Rowland, F. S.: Description of the analysis of a wide range of volatile organic compounds in whole air samples collected during PEM-Tropics A and B, *Anal. Chem.*, 73, 3723–3731, 2001.
- Cooper, O. R., Stohl, A., Hübner, G., Hsie, E. Y., Parrish, D. D., Tuck, A. F., Kiladis, G. N., Oltmans, S. J., Johnson, B. J., Shapiro, M., and Moody, J. L.: Direct transport of midlatitude stratospheric ozone into the lower troposphere and marine boundary layer of the tropical Pacific Ocean, *J. Geophys. Res.-Atmos.*, 110, D23310, <https://doi.org/10.1029/2005JD005783>, 2005.
- Crutzen, P.: A discussion of the chemistry of some minor constituents in the stratosphere and troposphere, *Pure Appl. Geophys.*, 106, 1385–1399, 1973.
- Derwent, R. G., Utembe, S. R., Jenkin, M. E., and Shallcross, D. E.: Tropospheric ozone production regions and the intercontinental origins of surface ozone over Europe, *Atmos. Environ.*, 112, 216–224, 2015.
- Ding, A., Wang, T., Xue, L., Gao, J., Stohl, A., Lei, H., Jin, D., Ren, Y., Wang, X., Wei, X., and Qi, Y.: Transport of north China air pollution by midlatitude cyclones: Case study of aircraft measurements in summer 2007, *J. Geophys. Res.-Atmos.*, 114, D08304, <https://doi.org/10.1029/2008JD011023>, 2009.
- Ding, A. J., Fu, C. B., Yang, X. Q., Sun, J. N., Zheng, L. F., Xie, Y. N., Herrmann, E., Nie, W., Petäjä, T., Kerminen, V.-M., and Kulmala, M.: Ozone and fine particle in the western Yangtze River Delta: an overview of 1 yr data at the SORPES station, *Atmos. Chem. Phys.*, 13, 5813–5830, <https://doi.org/10.5194/acp-13-5813-2013>, 2013.
- Duncan, B. N., Lamsal, L. N., Thompson, A. M., Yoshida, Y., Lu, Z., Streets, D. G., Hurwitz, M. M., and Pickering, K. E.: A space-based, high-resolution view of notable changes in urban NO_x pollution around the world (2005–2014), *J. Geophys. Res.-Atmos.*, 121, 976–996, 2016.
- Dunlea, E. J., Herndon, S. C., Nelson, D. D., Volkamer, R. M., San Martini, F., Sheehy, P. M., Zahniser, M. S., Shorter, J. H., Wormhoudt, J. C., Lamb, B. K., Allwine, E. J., Gaffney, J. S., Marley, N. A., Grutter, M., Marquez, C., Blanco, S., Cardenas, B., Retama, A., Ramos Villegas, C. R., Kolb, C. E., Molina, L. T., and Molina, M. J.: Evaluation of nitrogen dioxide chemiluminescence monitors in a polluted urban environment, *Atmos. Chem. Phys.*, 7, 2691–2704, <https://doi.org/10.5194/acp-7-2691-2007>, 2007.
- Finlayson-Pitts, B. J. and Pitts Jr., J. N.: Atmospheric chemistry of tropospheric ozone formation: scientific and regulatory implications, *Air Waste Manage. Assoc.*, 43, 1091–1100, 1993.
- Fung, J. C. H., Lau, A. K. H., Lam, J. S. L., and Yuan, Z.: Observational and modeling analysis of a severe air pollution episode in western Hong Kong, *J. Geophys. Res.-Atmos.*, 110, D09105, <https://doi.org/10.1029/2004JD005105>, 2005.
- Gao, J., Wang, T., Ding, A., and Liu, C.: Observational study of ozone and carbon monoxide at the summit of mount Tai (1534 m asl) in central-eastern China, *Atmos. Environ.*, 39, 4779–4791, 2005.
- Granby, K., Christensen, C. S., and Lohse, C.: Urban and semi-rural observations of carboxylic acids and carbonyls, *Atmos. Environ.*, 31, 1403–1415, 1997.
- Grosjean, D., Miguel, A. H., and Tavares, T. M.: Urban air pollution in Brazil: Acetaldehyde and other carbonyls, *Atmos. Environ.*, 24, 101–106, 1990.
- Gu, D., Wang, Y., Smeltzer, C., and Boersma, K. F.: Anthropogenic emissions of NO_x over China: Reconciling the difference of inverse modeling results using GOME-2 and OMI measurements, *J. Geophys. Res.-Atmos.*, 119, 7732–7740, 2014.
- Guo, H., Ling, Z. H., Cheung, K., Jiang, F., Wang, D. W., Simpson, I. J., Barletta, B., Meinardi, S., Wang, T. J., Wang, X. M., Saunders, S. M., and Blake, D. R.: Characterization of photochemical pollution at different elevations in mountainous areas in Hong Kong, *Atmos. Chem. Phys.*, 13, 3881–3898, <https://doi.org/10.5194/acp-13-3881-2013>, 2013.
- Han, X., Zhu, L., Wang, S., Meng, X., Zhang, M., and Hu, J.: Modeling study of impacts on surface ozone of regional transport and emissions reductions over North China Plain in summer 2015, *Atmos. Chem. Phys.*, 18, 12207–12221, <https://doi.org/10.5194/acp-18-12207-2018>, 2018.
- He, J., Wang, Y., Hao, J., Shen, L., and Wang, L.: Variations of surface O₃ in August at a rural site near Shanghai: influences from the West Pacific subtropical high and anthropogenic emissions, *Environ. Sci. Pollut. Res.*, 19, 4016–4029, 2012.
- He, K.: Multi-resolution Emission Inventory for China (MEIC): model framework and 1990–2010 anthropogenic emissions, in:

- AGU Fall Meeting Abstracts, 3–7 December 2012, San Francisco, 2012.
- Huang, J. P., Fung, J. C., Lau, A. K., and Qin, Y.: Numerical simulation and process analysis of typhoon-related ozone episodes in Hong Kong, *J. Geophys. Res.-Atmos.*, 110, D05301, <https://doi.org/10.1029/2004JD004914>, 2005.
- Jenkin, M. E. and Clemetshaw, K. C.: Ozone and other secondary photochemical pollutants: chemical processes governing their formation in the planetary boundary layer, *Atmos. Environ.*, 34, 2499–2527, 2000.
- Jenkin, M. E., Saunders, S. M., and Pilling, M. J.: The tropospheric degradation of volatile organic compounds: a protocol for mechanism development, *Atmos. Environ.*, 31, 81–104, 1997.
- Jiang, F., Guo, H., Wang, T. J., Cheng, H. R., Wang, X. M., Simpson, I. J., Ding, A. J., Saunders, S. M., Lam, S. H. M., and Blake, D. R.: An ozone episode in the Pearl River Delta: Field observation and model simulation, *J. Geophys. Res.-Atmos.*, 115, D22305, <https://doi.org/10.1029/2009JD013583>, 2010.
- Jin, X., Fiore, A. M., Murray, L. T., Valin, L. C., Lamsal, L. N., Duncan, B., Folkert Boersma, K., De Smedt, I., Abad, G. G., Chance, K., and Tonnesen, G. S.: Evaluating a Space-Based Indicator of Surface Ozone-NO_x-VOC Sensitivity Over Midlatitude Source Regions and Application to Decadal Trends, *J. Geophys. Res.-Atmos.*, 122, 10439–10461, 2017.
- Kanaya, Y., Pochanart, P., Liu, Y., Li, J., Tanimoto, H., Kato, S., Suthawaree, J., Inomata, S., Taketani, F., Okuzawa, K., Kawamura, K., Akimoto, H., and Wang, Z. F.: Rates and regimes of photochemical ozone production over Central East China in June 2006: a box model analysis using comprehensive measurements of ozone precursors, *Atmos. Chem. Phys.*, 9, 7711–7723, <https://doi.org/10.5194/acp-9-7711-2009>, 2009.
- Kleinman, L. I.: The dependence of tropospheric ozone production rate on ozone precursors, *Atmos. Environ.*, 3, 575–586, 2005.
- Kusaka, H. and Kimura, F.: Coupling a single-layer urban canopy model with a simple atmospheric model: Impact on urban heat island simulation for an idealized case, *J. Meteorol. Soc. Jpn. Ser. II*, 82, 67–80, 2004.
- Lam, S. H. M., Saunders, S. M., Guo, H., Ling, Z. H., Jiang, F., Wang, X. M., and Wang, T. J.: Modelling VOC source impacts on high ozone episode days observed at a mountain summit in Hong Kong under the influence of mountain-valley breezes, *Atmos. Environ.*, 81, 166–176, 2013.
- Lang, J., Zhang, Y., Zhou, Y., Cheng, S., Chen, D., Guo, X., Chen, S., Li, X., Xing, X., and Wang, H.: Trends of PM_{2.5} and chemical composition in Beijing, 2000–2015, *Aerosol Air Qual. Res.*, 17, 412–425, 2017.
- Li, M., Zhang, Q., Kurokawa, J.-I., Woo, J.-H., He, K., Lu, Z., Ohara, T., Song, Y., Streets, D. G., Carmichael, G. R., Cheng, Y., Hong, C., Huo, H., Jiang, X., Kang, S., Liu, F., Su, H., and Zheng, B.: MIX: a mosaic Asian anthropogenic emission inventory under the international collaboration framework of the MICS-Asia and HTAP, *Atmos. Chem. Phys.*, 17, 935–963, <https://doi.org/10.5194/acp-17-935-2017>, 2017.
- Lin, M., Fiore, A. M., Horowitz, L. W., Langford, A. O., Oltmans, S. J., Tarasick, D., and Rieder, H. E.: Climate variability modulates western US ozone air quality in spring via deep stratospheric intrusions, *Nat. Commun.*, 6, 7105, <https://doi.org/10.1038/ncomms8105>, 2015.
- Lin, M., Horowitz, L. W., Payton, R., Fiore, A. M., and Tonnesen, G.: US surface ozone trends and extremes from 1980 to 2014: quantifying the roles of rising Asian emissions, domestic controls, wildfires, and climate, *Atmos. Chem. Phys.*, 17, 2943–2970, <https://doi.org/10.5194/acp-17-2943-2017>, 2017.
- Lin, W., Xu, X., Zhang, X., and Tang, J.: Contributions of pollutants from North China Plain to surface ozone at the Shangdianzi GAW Station, *Atmos. Chem. Phys.*, 8, 5889–5898, <https://doi.org/10.5194/acp-8-5889-2008>, 2008.
- Liu, F., Beirle, S., Zhang, Q., van der A, R. J., Zheng, B., Tong, D., and He, K.: NO_x emission trends over Chinese cities estimated from OMI observations during 2005 to 2015, *Atmos. Chem. Phys.*, 17, 9261–9275, <https://doi.org/10.5194/acp-17-9261-2017>, 2017.
- Liu, X. H., Zhang, Y., Xing, J., Zhang, Q., Wang, K., Streets, D. G., Jang, C., Wang, W. X., and Hao, J. M.: Understanding of regional air pollution over China using CMAQ, part II. Process analysis and sensitivity of ozone and particulate matter to precursor emissions, *Atmos. Environ.*, 44, 3719–3727, 2010.
- Lo, J. C., Lau, A. K., Fung, J. C., and Chen, F.: Investigation of enhanced cross-city transport and trapping of air pollutants by coastal and urban land-sea breeze circulations, *J. Geophys. Res.-Atmos.*, 111, D14104, <https://doi.org/10.1029/2005JD006837>, 2006.
- Lu, K., Zhang, Y., Su, H., Brauers, T., Chou, C. C., Hofzumahaus, A., Liu, S. C., Kita, K., Kondo, Y., Shao, M., and Wahner, A.: Oxidant (O₃ + NO₂) production processes and formation regimes in Beijing, *J. Geophys. Res.-Atmos.*, 115, D07303, <https://doi.org/10.1029/2009JD012714>, 2010.
- Lyu, X.: Data for the paper “Causes of a continuous summertime O₃ pollution event in Jinan, a central city in the North China Plain”, Google Drive, available at: https://drive.google.com/open?id=1_KeOxOuVsLY83xL74RtcRORsiiyIR8FZ, 2018.
- Lyu, X. P., Chen, N., Guo, H., Zhang, W. H., Wang, N., Wang, Y., and Liu, M.: Ambient volatile organic compounds and their effect on ozone production in Wuhan, central China, *Sci. Total Environ.*, 541, 200–209, 2016.
- Lyu, X. P., Guo, H., Wang, N., Simpson, I. J., Cheng, H. R., Zeng, L. W., Saunders, S. M., Lam, S. H. M., Meinardi, S., and Blake, D. R.: Modeling C₁–C₄ alkyl nitrate photochemistry and their impacts on O₃ production in urban and suburban environments of Hong Kong, *J. Geophys. Res.-Atmos.*, 122, 10539–10556, 2017.
- Madronich, S. and Flocke, S.: Theoretical estimation of biologically effective UV radiation at the Earth’s surface, in: *Solar Ultraviolet Radiation*, Springer, Berlin, Heidelberg, 23–48, 1997.
- Mao, J., Ren, X., Chen, S., Brune, W. H., Chen, Z., Martinez, M., Harder, H., Lefer, B., Rappenglueck, B., Flynn, J., and Leuchner, M.: Atmospheric oxidation capacity in the summer of Houston 2006: Comparison with summer measurements in other metropolitan studies, *Atmos. Environ.*, 44, 4107–4115, 2010.
- McCleny, W. A., Williams, E. J., Cohen, R. C., and Stutz, J.: Preparing to measure the effects of the NO_x SIP Call – methods for ambient air monitoring of NO, NO₂, NO_y, and individual NO_z species, *Air Waste Manage. Assoc.*, 52, 542–562, 2002.
- Monks, P. S.: Gas-phase radical chemistry in the troposphere, *Chem. Soc. Rev.*, 34, 376–395, 2005.
- Ren, X., Harder, H., Martinez, M., Lesher, R. L., Olinger, A., Simpas, J. B., Brune, W. H., Schwab, J. J., Demerjian, K. L., He, Y., and

- Zhou, X.: OH and HO₂ chemistry in the urban atmosphere of New York City, *Atmos. Environ.*, 37, 3639–3651, 2003.
- Saunders, S. M., Jenkin, M. E., Derwent, R. G., and Pilling, M. J.: Protocol for the development of the Master Chemical Mechanism, MCM v3 (Part A): tropospheric degradation of non-aromatic volatile organic compounds, *Atmos. Chem. Phys.*, 3, 161–180, <https://doi.org/10.5194/acp-3-161-2003>, 2003.
- Shan, W., Yin, Y., Zhang, J., and Ding, Y.: Observational study of surface ozone at an urban site in East China, *Atmos. Res.*, 89, 252–261, 2008.
- Shao, M., Lu, S., Liu, Y., Xie, X., Chang, C., Huang, S., and Chen, Z.: Volatile organic compounds measured in summer in Beijing and their role in ground-level ozone formation, *J. Geophys. Res.-Atmos.*, 114, D00G06, <https://doi.org/10.1029/2008JD010863>, 2009.
- Shu, L., Xie, M., Wang, T., Gao, D., Chen, P., Han, Y., Li, S., Zhuang, B., and Li, M.: Integrated studies of a regional ozone pollution synthetically affected by subtropical high and typhoon system in the Yangtze River Delta region, China, *Atmos. Chem. Phys.*, 16, 15801–15819, <https://doi.org/10.5194/acp-16-15801-2016>, 2016.
- Sillman, S.: The relation between ozone, NO_x and hydrocarbons in urban and polluted rural environments, *Atmos. Environ.*, 33, 1821–1845, 1999.
- Sun, L., Xue, L., Wang, T., Gao, J., Ding, A., Cooper, O. R., Lin, M., Xu, P., Wang, Z., Wang, X., Wen, L., Zhu, Y., Chen, T., Yang, L., Wang, Y., Chen, J., and Wang, W.: Significant increase of summertime ozone at Mount Tai in Central Eastern China, *Atmos. Chem. Phys.*, 16, 10637–10650, <https://doi.org/10.5194/acp-16-10637-2016>, 2016.
- Tan, Z., Lu, K., Dong, H., Hu, M., Li, X., Liu, Y., Lu, S., Shao, M., Su, R., Wang, H., and Wu, Y.: Explicit diagnosis of the local ozone production rate and the ozone-NO_x-VOC sensitivities, *Sci. Bull.*, 63, 1067–1076, 2018a.
- Tan, Z., Lu, K., Jiang, M., Su, R., Dong, H., Zeng, L., Xie, S., Tan, Q., and Zhang, Y.: Exploring ozone pollution in Chengdu, southwestern China: A case study from radical chemistry to O₃-VOC-NO_x sensitivity, *Sci. Total Environ.*, 636, 775–786, 2018b.
- Thornton, J. A., Wooldridge, P. J., Cohen, R. C., Martinez, M., Harder, H., Brune, W. H., Williams, E. J., Roberts, J. M., Fehsenfeld, F. C., Hall, S. R., and Shetter, R. E.: Ozone production rates as a function of NO_x abundances and HO_x production rates in the Nashville urban plume, *J. Geophys. Res.-Atmos.*, 107, 4146, <https://doi.org/10.1029/2001JD000932>, 2002.
- Wang, N., Guo, H., Jiang, F., Ling, Z. H., and Wang, T.: Simulation of ozone formation at different elevations in mountainous area of Hong Kong using WRF-CMAQ model, *Sci. Total Environ.*, 505, 939–951, 2015.
- Wang, T., Ding, A., Gao, J., and Wu, W. S.: Strong ozone production in urban plumes from Beijing, China, *Geophys. Res. Lett.*, 33, L21806, <https://doi.org/10.1029/2006GL027689>, 2006.
- Wang, T., Nie, W., Gao, J., Xue, L. K., Gao, X. M., Wang, X. F., Qiu, J., Poon, C. N., Meinardi, S., Blake, D., Wang, S. L., Ding, A. J., Chai, F. H., Zhang, Q. Z., and Wang, W. X.: Air quality during the 2008 Beijing Olympics: secondary pollutants and regional impact, *Atmos. Chem. Phys.*, 10, 7603–7615, <https://doi.org/10.5194/acp-10-7603-2010>, 2010.
- Wang, X. M., Lin, W. S., Yang, L. M., Deng, R. R., and Lin, H.: A numerical study of influences of urban land-use change on ozone distribution over the Pearl River Delta region, China, *Tellus B*, 59, 633–641, 2007.
- Wang, Z., Li, Y., Chen, T., Zhang, D., Sun, F., Wei, Q., Dong, X., Sun, R., Huan, N., and Pan, L.: Ground-level ozone in urban Beijing over a 1-year period: Temporal variations and relationship to atmospheric oxidation, *Atmos. Res.*, 164, 110–117, 2015.
- Whitten, G. Z., Heo, G., Kimura, Y., McDonald-Buller, E., Allen, D. T., Carter, W. P., and Yarwood, G.: A new condensed toluene mechanism for Carbon Bond: CB05-TU, *Atmos. Environ.*, 44, 5346–5355, 2010.
- Williams, J., Kefel, S. U., Nölscher, A. C., Yang, Y., Lee, Y., Yáñez-Serrano, A. M., Wolff, S., Kesselmeier, J., Klüpfel, T., Lelieveld, J., and Shao, M.: Opposite OH reactivity and ozone cycles in the Amazon rainforest and megacity Beijing: Subversion of biospheric oxidant control by anthropogenic emissions, *Atmos. Environ.*, 125, 112–118, 2016.
- Xing, C., Liu, C., Wang, S., Chan, K. L., Gao, Y., Huang, X., Su, W., Zhang, C., Dong, Y., Fan, G., Zhang, T., Chen, Z., Hu, Q., Su, H., Xie, Z., and Liu, J.: Observations of the vertical distributions of summertime atmospheric pollutants and the corresponding ozone production in Shanghai, China, *Atmos. Chem. Phys.*, 17, 14275–14289, <https://doi.org/10.5194/acp-17-14275-2017>, 2017.
- Xing, J., Ding, D., Wang, S., Zhao, B., Jang, C., Wu, W., Zhang, F., Zhu, Y., and Hao, J.: Quantification of the enhanced effectiveness of NO_x control from simultaneous reductions of VOC and NH₃ for reducing air pollution in the Beijing–Tianjin–Hebei region, China, *Atmos. Chem. Phys.*, 18, 7799–7814, <https://doi.org/10.5194/acp-18-7799-2018>, 2018.
- Xu, Z., Wang, T., Xue, L. K., Louie, P. K., Luk, C. W., Gao, J., Wang, S. L., Chai, F. H., and Wang, W. X.: Evaluating the uncertainties of thermal catalytic conversion in measuring atmospheric nitrogen dioxide at four differently polluted sites in China, *Atmos. Environ.*, 76, 221–226, 2013.
- Xue, L. K., Wang, T., Gao, J., Ding, A. J., Zhou, X. H., Blake, D. R., Wang, X. F., Saunders, S. M., Fan, S. J., Zuo, H. C., Zhang, Q. Z., and Wang, W. X.: Ground-level ozone in four Chinese cities: precursors, regional transport and heterogeneous processes, *Atmos. Chem. Phys.*, 14, 13175–13188, <https://doi.org/10.5194/acp-14-13175-2014>, 2014.
- Yang, Y., Shao, M., Wang, X., Nölscher, A. C., Kessel, S., Guenther, A., and Williams, J.: Towards a quantitative understanding of total OH reactivity: A review, *Atmos. Environ.*, 134, 147–161, 2016.
- Ye, L., Wang, X., Fan, S., Chen, W., Chang, M., Zhou, S., Wu, Z., and Fan, Q.: Photochemical indicators of ozone sensitivity: application in the Pearl River Delta, China, *Front. Environ. Sci. Eng.*, 10, 15, <https://doi.org/10.1007/s11783-016-0887-1>, 2016.
- Yin, Y., Lu, H., Shan, W., and Zheng, Y.: Analysis of observed ozone episode in urban Jinan, China, *Bulletin Environ. Contam. Toxicol.*, 83, 159–163, 2009.
- Zhang, Q., Streets, D. G., He, K., Wang, Y., Richter, A., Burrows, J. P., Uno, I., Jang, C. J., Chen, D., Yao, Z., and Lei, Y.: NO_x emission trends for China, 1995–2004: The view from the ground and the view from space, *J. Geophys. Res.-Atmos.*, 112, D22306, <https://doi.org/10.1029/2007JD008684>, 2007.
- Zhang, Q., Streets, D. G., Carmichael, G. R., He, K. B., Huo, H., Kannari, A., limont, Z., Park, I. S., Reddy, S., Fu, J. S., Chen, D., Duan, L., Lei, Y., Wang, L. T., and Yao, Z. L.: Asian emissions

- in 2006 for the NASA INTEX-B mission, *Atmos. Chem. Phys.*, 9, 5131–5153, <https://doi.org/10.5194/acp-9-5131-2009>, 2009.
- Zhang, Q., Yuan, B., Shao, M., Wang, X., Lu, S., Lu, K., Wang, M., Chen, L., Chang, C.-C., and Liu, S. C.: Variations of ground-level O₃ and its precursors in Beijing in summertime between 2005 and 2011, *Atmos. Chem. Phys.*, 14, 6089–6101, <https://doi.org/10.5194/acp-14-6089-2014>, 2014.
- Zhang, Y., Ding, A., Mao, H., Nie, W., Zhou, D., Liu, L., Huang, X., and Fu, C.: Impact of synoptic weather patterns and inter-decadal climate variability on air quality in the North China Plain during 1980–2013, *Atmos. Environ.*, 124, 119–128, 2016.
- Zhang, Z., Zhang, X., Gong, D., Quan, W., Zhao, X., Ma, Z., and Kim, S. J.: Evolution of surface O₃ and PM_{2.5} concentrations and their relationships with meteorological conditions over the last decade in Beijing, *Atmos. Environ.*, 108, 67–75, 2015.
- Zhao, C., Wang, Y., and Zeng, T.: East China plains: A “basin” of ozone pollution, *Environ. Sci. Technol.*, 43, 1911–1915, 2009.
- Zheng, B., Tong, D., Li, M., Liu, F., Hong, C., Geng, G., Li, H., Li, X., Peng, L., Qi, J., Yan, L., Zhang, Y., Zhao, H., Zheng, Y., He, K., and Zhang, Q.: Trends in China’s anthropogenic emissions since 2010 as the consequence of clean air actions, *Atmos. Chem. Phys.*, 18, 14095–14111, <https://doi.org/10.5194/acp-18-14095-2018>, 2018.
- Zong, R., Yang, X., Wen, L., Xu, C., Zhu, Y., Chen, T., Yao, L., Wang, L., Zhang, J., Yang, L., Wang, X., Shao, M., Zhu, T., Xue, L., and Wang, W.: Strong ozone production at a rural site in the North China Plain: Mixed effects of urban plumes and biogenic emissions, *J. Environ. Sci.*, 71, 261–270, <https://doi.org/10.1016/j.jes.2018.05.003>, 2018.